THE ASTROPHYSICAL JOURNAL, 522:1108–1116, 1999 September 10

CORONAL TRAPPING OF ENERGETIC FLARE PARTICLES: *YOHKOH*/HXT OBSERVATIONS

THOMAS R. METCALF AND DAVID ALEXANDER
Lockheed Martin Solar and Astrophysics Laboratory, Department L9-41, Building 252, 3251 Hanover Street, Palo Alto, CA 94304;
metcalf@lmsal.com
Received 1998 November 24; accepted 1999 April 21

ABSTRACT

We examine spectroscopic data from the *Yohkoh* Hard X-Ray Telescope in a search for spectral evidence of the coronal trapping of energetic particles during solar flares. Two distinct particle populations with significantly different spectral properties are found to be present in three of the six flares studied; the first population is trapped in the corona, where it encounters a "thick-thin" target, while the second population precipitates directly to the footpoints. In the remaining three events, a single population of energetic particles appear to be responsible for the observed hard X-ray emission, either via thermal bremsstrahlung (one case) or nonthermal thin-target emission (two cases). For the three events in which a trapped population is observed, the spectroscopic observations imply first that there is likely to be a single acceleration mechanism for both the trapped and the precipitating populations and second that the magnetic field geometry in these flares is conducive to trapping in a confined region high in the corona, above the soft X-ray loops. Both conditions are consistent with magnetic reconnection models of flares in which energetic particles are trapped between MHD slow-mode shocks attached to the reconnection region and a fast-mode shock formed by the reconnection outflow jet.

Subject headings: acceleration of particles — Sun: corona — Sun: flares — Sun: X-rays, gamma rays

1. INTRODUCTION

Hard X-ray (HXR) emission from solar flares provides a crucial diagnostic in understanding the energization of the solar corona. The most common interpretation for the production of the observed HXR fluxes is bremsstrahlung from an energetic population of electrons accelerated in the flare. Thus, an understanding of the HXR emission provides information on the acceleration mechanism responsible for the production of the energetic particles. However, because the energetic particles propagate through a magnetized plasma, transport effects can alter the spectroscopic properties of the energetic particle distribution prior to bremsstrahlung production. To understand how the HXR observations relate to the particle acceleration, we must therefore understand the modification of the energetic particle spectrum as the particles propagate away from the acceleration site.

Many processes can affect the distribution of the particles in space (e.g., pitch angle scattering) and in energy (e.g., Coulomb collisions), and these have a marked effect on the production of photons, affecting total flux, spectral shape, and spatial location of emission. However, for typical coronal densities ($n \simeq 10^{10}$ cm^{-3}) and HXR-producing electron energies ($E \leq 100$ keV), the coronal transit time is very much shorter than the collision/scattering times (neglecting the presence of enhanced scattering due to waves), and so the corona can only have a major impact on the particle distribution if the particles remain in the corona for longer than typical loop transit times, i.e., via coronal trapping.

There is considerable evidence for the trapping of energetic particles in solar flares (e.g., Bai & Ramaty 1979; Bai et al. 1983; Bai & Dennis 1985; Ramaty et al. 1994). Recently, Aschwanden et al. (1996a) determined time delays in HXR pulses observed with the *Compton Gamma Ray Observatory* (*CGRO*) and interpreted these time delays as time-of-flight effects. In many of the flares studied, the time delays implied two distinct particle populations: fast burstlike time structures, interpreted as electrons that directly precipitate to the footpoints, yielded positive time delays, while smooth time structures, interpreted as electrons that are trapped for a time before precipitating, yielded negative time delays (Aschwanden et al. 1996a, 1997, respectively). However, such time-delay observations are ambiguous, because the time delays can also be interpreted as a two-step acceleration process or as time-dependent spectra occurring naturally as part of the acceleration process (Brown, Conway, & Aschwanden 1998).

The ambiguity between the time dependence of electron acceleration and a spectral modification in the corona, e.g., in a coronal trap, can be resolved by including spatially resolved HXR observations such as those from the *Yohkoh* Hard X-ray Telescope (HXT; Kosugi et al. 1991). Even in the presence of a time-dependent electron acceleration, spatial differentiation of the corona and chromosphere allows a measurement of any spectral modification as the electrons traverse the corona. Therefore, the observation of a spectral modification, through the comparison of the coronal and chromospheric spectra, implies the presence of trapping or a similar mechanism, independent of the complexities of the acceleration process. The spatial and spectral resolution of the HXT allows us to study coronal trapping by observing the local modification, if any, of the HXR energy spectrum.

Further, the combination of time-of-flight and spatially resolved spectral observations may yield considerable information on the acceleration mechanism. For example, if the local modification of the particle spectrum indicates that a trap is present, then observed time delays are likely due to time-of-flight effects from a trapped population rather than being an intrinsic property of the acceleration process itself.

In a recent study of the so-called Masuda flare (1993 January 13; Masuda et al. 1994, 1995), Alexander & Metcalf (1997, hereafter AM97) observed the modification of the energetic particle spectrum as electrons propagated into and through a coronal trap for which the weak diffusion

limit applied (Kennel & Petschek 1966). This confirmed, for a single event, the time-of-flight results of Aschwanden et al. (1997). In this paper we repeat this analysis for several more flares to determine whether coronal trapping is a ubiquitous phenomenon.

When electrons are trapped in the corona, the energy spectrum of the electrons is modified to an extent dependent on the trapping time (discussed in the Appendix). In the weak diffusion limit adopted here, the trapping time is governed by the particle deflection time (see MacKinnon 1988; Alexander 1990) and, consequently, is proportional to a positive power of the energy. Thus, higher energy electrons remain in the trap longer, resulting in a spectrum in the trap that hardens with time. For the 1992 January 13 flare presented by AM97, the HXT observations were consistent with this scenario if the coronal trap also acts a thick-thin target (Wheatland & Melrose 1995) in which the corona presents a thick target to lower energy electrons and a thin target to higher energy electrons.

The surprising discovery from the HXT of HXR emission *above* the coronal portion of a flaring loop (Masuda et al. 1994, 1995) was thereby understood to result from a population of electrons trapped locally in the corona. Such a scenario is predicted by the magnetic reconnection model of flares (e.g., Masuda et al. 1994; Shibata et al. 1995; Tsuneta et al. 1997). In this model, MHD slow-mode shocks attached to the reconnection region convert magnetic energy into plasma heating and an outflow jet. The outflow jet forms a fast-mode shock just above the loop-top HXR source, creating a region between the slow-mode and fast-mode shocks where energetic electrons are trapped. In a recent elaboration of this model, Tsuneta & Naito (1998) demonstrate how electrons can be accelerated through a first-order Fermi process at the fast shock. Hence, observations of the coronal trap above the soft X-ray (SXR) loop may be intimately connected with the particle acceleration process itself.

In this work, we examine six solar limb flares observed with HXT to determine whether the HXR source above the SXR loop in the 1992 January 13 flare was unique or similar transport effects can be observed in many flares.

2. OBSERVATIONS AND ANALYSIS

The HXT data selected for this study all show a clear coronal HXR signature (e.g., Masuda et al. 1994, 1995), as well as distinct footpoint emission (Figs. 1 and 2). Three of the events selected were also included in the Aschwanden et al. (1996b) time-of-flight study.

HXT images were reconstructed using the Pixon method described by Metcalf et al. (1996). The Pixon algorithm is a maximum entropy method (MEM), with the refinement that the reconstructed "pixels" are allowed to vary in size over the image in proportion to the information content of the image at each location. As shown by AM97, the Pixon method has the advantage of providing better noise suppression and hence better photometry than the standard MEM reconstructions. For a spectral analysis defined by channel ratios, as used in this paper, it is important to use the best possible photometry. The image reconstructions computed for this study also incorporate the latest HXT response functions (Sato, Kosugi, & Makishima 1998) for

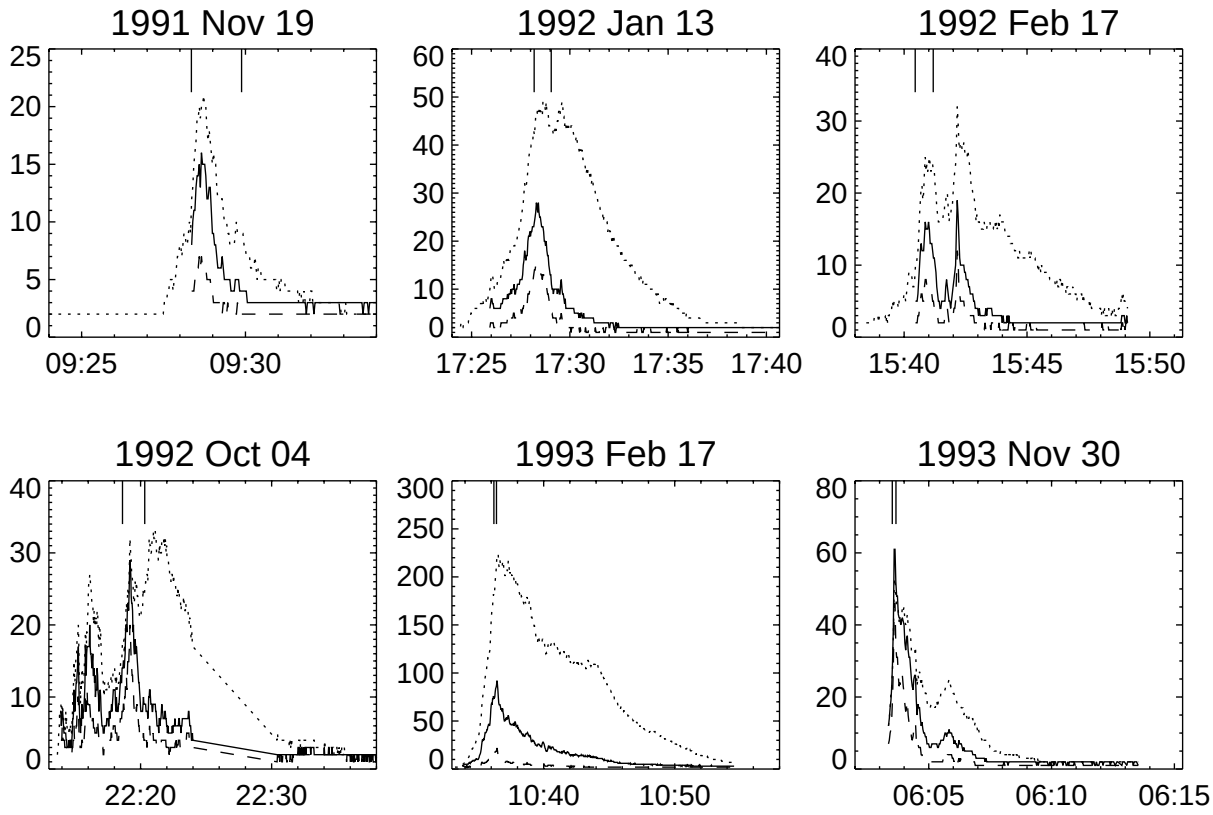

FIG. 1.—HXR light curves for the six events studied. The vertical bars at the top show the time integrations used for each event. The later peak in the 1992 February 17 flare and the earlier peak in the 1992 October 4 flare did not have enough counts for a reliable image reconstruction. The dashed line shows the M2 emission, while the solid and dotted lines show the M1 and LO emission, respectively.

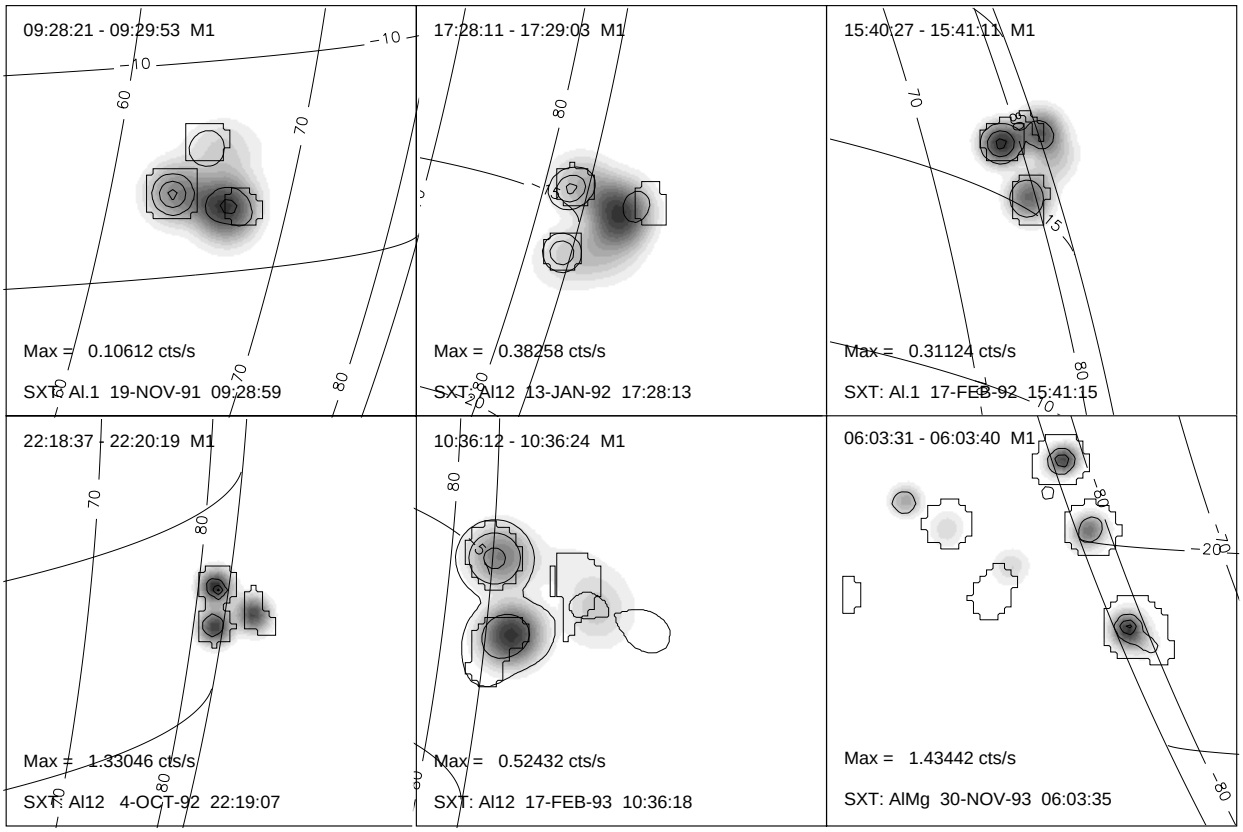

FIG. 2.—Six events studied. The underlying images are from the *Yohkoh* Soft X-Ray Telescope (SXT), the thick contours are from the HXT M1 channel (15%, 50%, and 90% of the maximum emission) at the time of the peak in the M1 emission, and the thin contours show the spatial integration boxes (M2 contours) for the corona and the footpoints of the flares. The grids show the solar latitude and CMD. In each case, the field-of-view is 64 SXT pixels (2.″46) with solar north up and solar east to the left.

all HXT channels.[1] The incorporation of the new response functions, together with the correction of the flux-estimation algorithm (Sato et al. 1998), signifies a substantial improvement in the image deconvolution of HXT data.

For each flare in this study, we derived HXR impulsive-phase spectral parameters for the flare footpoints and coronal sources using ratios of the HXT energy channels (primarily LO/M1 and M1/M2). To isolate the coronal and footpoint sources, a perimeter is drawn around each source, and the HXR emission within each perimeter is summed for each energy channel. To eliminate possible contamination by the thermal plasma in the SXR loop, the selection of pixels for inclusion in the spatial summation is further restricted by including only those pixels within the perimeter containing significant HXR emission in the M2 channel (the perimeter is defined to be the 30% contour of the M2 emission in each localized region, which minimizes the inclusion of spurious sources but includes all relevant emission). The channel ratios used in the calculation of the spectral parameters are ratios of these summed emissions. The perimeters and integration periods are identical for each channel used in the ratios.

Figures 1 and 2 show the soft and HXR observations of the six flares studied. All flares are on or close to the limb and most show clear evidence of HXR emission *above* the SXR loops. Most of the events exhibit a relatively simple loop geometry and strong HXR footpoints are clear in all cases. However, the flares of 1993 February 17 and November 30 show a more complicated structure, with perhaps multiple loops participating in the flare.

The calculation of the spectral parameters is carried out using the method of AM97. For the footpoints, we assume that the HXR emission is thick target bremsstrahlung resulting from the injection of energetic electrons with a power-law energy spectrum and derive a spectral index from this model. For the coronal sources, we derive both thin- and thick-target nonthermal power-law spectral indices, as well as a temperature assuming a thermal model of the HXR emission. The calculation of the HXR spectral parameters includes the transmission efficiency of the HXT filter, the pulse-height distribution of the detector, and the K-escape modification of Takakura et al. (1993; see Fig. 7 of AM97). The results of the spectral analysis are presented in Table 1. In all cases, the numbers quoted were derived at the peak of the impulsive phase as determined from the M1 channel emission (Fig. 1).

Table 1 shows the spectral parameters of each flare from both the LO/M1 and the M1/M2 channel ratios. The value $\delta_{\rm inj}$ gives the electron spectral index inferred from the footpoints of the flare and is assumed to indicate the spectrum of the electrons injected into the corona (discussed further below). The parameters $\delta_{\rm corona}^{\rm thick}$ and $\delta_{\rm corona}^{\rm thin}$ show the electron spectral indices of the coronal source in the thick- and thin-

[1] LO: 13.9–22.7 keV; M1: 22.7–32.7 keV; M2: 32.7–52.7 keV; HI: 52.7–92.8 keV

TABLE 1

HXT OBSERVATIONS: SPECTRAL PARAMETERS

Date	Ratio	δ_{inj}	δ^{thick}_{corona}	δ^{thin}_{corona}	T_{corona} (MK)	Trap?
1991 Nov 19.....	LO/M1	4.3 ± 0.3	6.3 ± 0.3	**4.3 ± 0.3**	58 ± 4	
09:29 UT	M1/M2	5.9 ± 0.3	7.4 ± 0.6	**5.4 ± 0.6**	...	No
1992 Jan 13.....	LO/M1	4.3 ± 0.1	**3.2 ± 0.6**	...	215 ± 60	
17:27 UT	M1/M2	4.5 ± 0.1	5.1 ± 0.2	**3.1 ± 0.2**	120 ± 15	Yes
1992 Feb 17	LO/M1	4.7 ± 0.1	7.5 ± 0.3	**5.5 ± 0.3**	58 ± 6	
17:27 UT	M1/M2	5.3 ± 0.1	8.0 ± 0.7	**6.0 ± 0.7**	44 ± 2	No
1992 Oct 04	LO/M1	4.4 ± 0.1	10.2 ± 8	8.2 ± 8	**27 ± 2**	
22:19 UT	M1/M2	4.4 ± 0.1	10.3 ± 8	8.3 ± 8	**39 ± 11**	No
1993 Feb 17	LO/M1	6.2 ± 0.2	6.5 ± 1.4	**4.5 ± 1.4**	45 ± 10	
10:36 UT	M1/M2	6.4 ± 0.2	7.4 ± 1.3	**5.4 ± 1.3**	31 ± 5	Yes
1993 Nov 30.....	LO/M1	4.0 ± 0.2	**2.2 ± 1.1**	...	...	
06:04 UT	M1/M2	4.5 ± 0.2	4.0 ± 0.5	**2.0 ± 0.5**	...	Yes

target interpretations, respectively. From the observed photon spectral index in the corona, we derive the electron spectral index under both the assumption of a thin (δ^{thin}_{corona}) and thick (δ^{thick}_{corona}) target. By definition, $\delta^{thick}_{corona} = \delta^{thin}_{corona} + 2$. The temperature (MK) of the coronal source assuming a thermal model is indicated by T_{corona}. Finally, the last column indicates whether the spectral parameters of the event are consistent with the trapping hypothesis. The boldface coronal spectral indices in Table 1 show whether we consider the data to be best fitted by a thick-thin or thin-target coronal model. Note that a thin-thick model is rejected on physical grounds because the corona cannot be thinner to lower energy electrons than to higher energy electrons. In a few cases, a channel ratio was inconsistent with the thin-target (integrated energy is infinite) or thermal model (M2 counts greater than M1 counts), resulting in the rejection of that model for that flare. These cases are indicated in Table 1 by ellipses.

The errors on the spectral indices quoted in Table 1 were derived from errors determined in the HXT image reconstruction, which, in turn, were derived from the statistical errors on the HXT data. After the reconstruction, each pixel is given a count rate error estimate, and these are folded through the spatial integration and the spectral analysis. It should be noted, however, that these errors do not give any meaningful measure on how well the reconstructed images represent the "true" distribution of emission.

The problem of accounting for errors in the selection of the particular reconstruction used is difficult, because a single pixel is not very well constrained by the data. Most images that one might use to determine such errors are not valid images; a perturbation in one pixel does not in general yield a valid reconstruction. The correct approach to this problem would utilize the Bayesian probabilities (see Metcalf et al. 1996) to define a range of acceptable reconstructions. However, this is intractable because of the enormous computing times involved. This should not, however, be construed as a serious problem. The robustness of the Pixon method gives us confidence that the image reconstruction is a fair representation of the distribution of HXR emission. Because the reconstruction is robust, the errors quoted in Table 1, derived from the counting statistics of the data, are also robust.

There were several spectral properties of the HXR emission in the Masuda flare, which led AM97 to conclude that coronal trapping could explain the coronal HXR source. Our goal here is to look for similar properties in coronal sources seen in other flares. First, because the coronal trapping time in the weak diffusion limit is proportional to a positive power of the electron energy, the average inferred spectrum determined from the coronal trap is harder than the injected spectrum.[2] Second, the thermal model was rejected because it was not possible to compute a consistent temperature between the various channel ratios. Finally, the coronal trap was observed to act as a thick target to lower energy electrons and a thin target to higher energy electrons.

To compare the inferred spectrum in the coronal source with the injected spectrum obviously requires a measure of the injected spectrum. We follow AM97 and assume that the spectrum of the injected electrons is the same as the electron spectrum inferred from the footpoint emission (as in AM97, both footpoints are treated as a single source). This is justified when the precipitating electrons are assumed to have propagated through the trap (either directly precipitating electrons or trapped electrons that have scattered into the loss cone of the coronal trap). For a continuous injection of electrons into the trapping region, the precipitating electrons will have the same spectrum as the injected electrons once a trapping time (for high-energy electrons) has passed, even if these electrons have been trapped before scattering into the loss cone. This is also the case for impulsively injected electrons if the data accumulation time is longer than a trapping time for higher energy electrons.

The only caveat to the assumption that the footpoint spectrum reflects the spectrum of the injected electrons is that the spectrum will be modified in the trap if the trap column density is sufficiently large. This would primarily be a hardening of the spectrum when lower energy electrons see a "thicker" target than higher energy electrons. Hence the footpoint spectral index is a lower limit to the injected spectral index. However, in the trap-precipitation events, we expect any spectrum modifications to be important only for the trapped electrons that see a larger coronal column depth than the directly precipitating electrons ($N_{trap}/N_{direct} \propto t_{trap}/t_{bounce}$) before being scattered into the loss cone.

[2] In the Appendix we demonstrate that the inferred spectrum determined from the coronal trap is harder than the injected spectrum by a power of ~ 1.5 when the injection of particles is continuous over a time longer than the trapping time or when the data accumulation time is greater than the trapping time.

We consider two general cases of coronal trapping in the weak diffusion limit and suggest spectral effects observable with HXT data. This division into two cases is based on the relative magnitudes of the trapping time and the data accumulation time. The details of the modification of the electron spectra in the trap are discussed in the Appendix (see Figs. 3 and 4). Because of the long integration times required for HXT imaging, the *short trapping time* case is the norm.

Short Trapping Time.—When the trapping time is short compared with the data accumulation time, the average inferred spectrum in the coronal trap is harder than the injected spectrum by a power of ~ 1.5, as found in the 1992 January 13 Masuda flare. This is demonstrated in the Appendix. The result holds both for a continuous (injection timescale long compared with the trapping time) and an impulsive (injection timescale short compared with the trapping time) injection of electrons into the trap. In the impulsive case, the inferred spectrum of the electrons in the trap is harder because the higher energy electrons remain in the trap longer and produce more emission, even though all electrons escape the trap during a single data accumulation time.

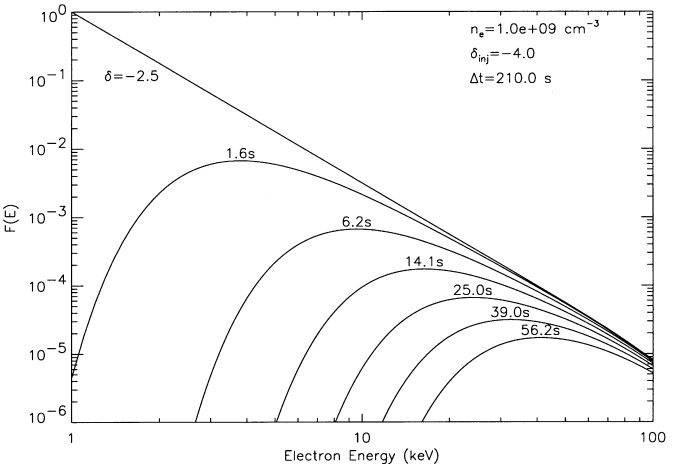

FIG. 3.—Evolution of the observed spectrum with time after the impulsive injection of electrons into a coronal trap for the case of a long accumulation time. The injected spectrum has a spectral index of 4; the diagonal line shows the limiting spectrum hardened by 1.5 powers (2.5).

Long Trapping Time.—In this case, the inferred spectrum of the electrons in the trap is identical to the injected distribution, as very few particles escape over a single data accumulation time. Over time, if the observation lasts long enough, the spectrum would appear to harden as the lower energy electrons escape the trap before the higher energy electrons. Again, this result holds for both impulsive and continuous injection of electrons into the trap.

Table 2 summarizes the spectral effects of various acceleration/coronal trap scenarios in the weak diffusion limit. The value Δt_{inj} is the time over which electrons are injected into the trap, Δt_{trap} is the trapping time, and Δt_{data} is the data accumulation time; δ_{inj} is the spectral index of the electrons injected into the trap, while δ_{corona} is the inferred spectral index for the trapped electrons. A right arrow represents time evolution of the spectral indices. When $\Delta t_{trap} > \Delta t_{data}$, a coronal trap is indicated by the temporal hardening of the electron spectrum from an initial value of δ_{inj} to a value of $\delta_{inj} - 3/2$. However, when $\Delta t_{trap} < \Delta t_{data}$, as for HXT, a coronal trap is indicated by a coronal spectral index of $\delta_{inj} - 3/2$.

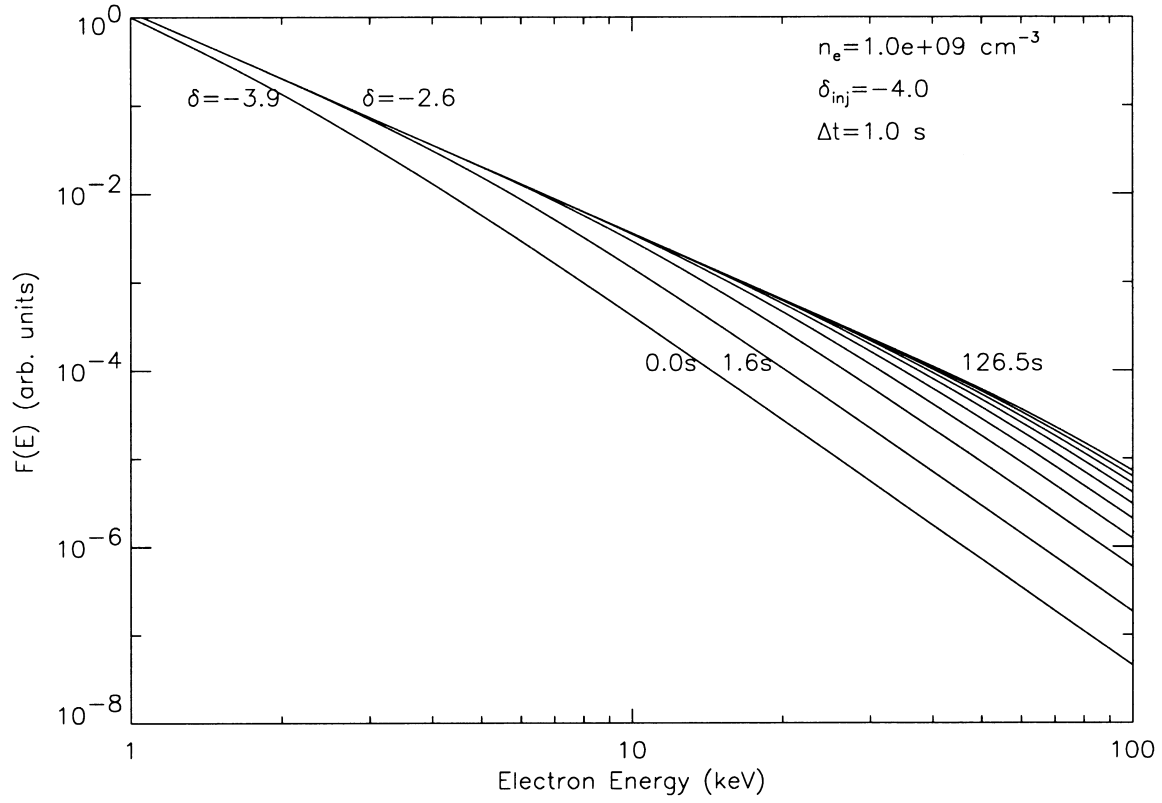

FIG. 4.—Evolution of the observed spectrum with time with the continuous injection of electrons into a coronal trap

TABLE 2

CORONAL TRAPS: HXR SPECTRAL EFFECTS IN THE WEAK DIFFUSION LIMIT

Model	Injection Profile	$\delta_{\rm trap}$
$\Delta t_{\rm inj} > \Delta t_{\rm data} > \Delta t_{\rm trap}$	Continuous	$\delta_{\rm inj} - 3/2$
$\Delta t_{\rm inj} > \Delta t_{\rm trap} > \Delta t_{\rm data}$	Continuous	$\delta_{\rm inj} \rightarrow \delta_{\rm inj} - 3/2$
$\Delta t_{\rm inj} < \Delta t_{\rm trap} < \Delta t_{\rm data}$	Impulsive[a]	$\delta_{\rm inj} - 3/2$
$\Delta t_{\rm inj} < \Delta t_{\rm data} < \Delta t_{\rm trap}$	Impulsive[a]	$\delta_{\rm inj} \rightarrow \delta_{\rm inj} - 3/2$

NOTE.—Right arrow indicates temporal development.

[a] Energy cutoff moves to higher energy with time.

The thick-thin target observed in the Masuda flare by AM97, in which the trap acts as a thick target to lower energy electrons and a thin target to higher energy electrons, complicates the interpretation of the data as it may or may not be present in other flares. The trap could be thick-thin, thick-, or thin-target, depending on the column depth of the trap.

If the trap is thick-thin, as observed in the 1992 January 13 flare, the LO/M1 electron spectral index given by $\delta^{\rm thick}_{\rm corona}$ will equal the M1/M2 electron spectral index given by $\delta^{\rm thin}_{\rm corona}$. In a standard thick- or thin-target scenario both channel ratios would yield the same spectral index in either the thick or thin target scenario. Consequently, the thick- and thin-target models can only be distinguished through a comparison with the injected spectral index. The model that best fits the data is indicated in Table 1 by boldface equivalent spectral indices for each channel ratio. For example, the bold values for the 1992 January 13 event indicate that the thick-thin model best fits the data. For the long data accumulation times used with HXT, the spectral indices of the coronal source will be 1.5 powers harder than the injected spectrum when a trap is present. To conclude that a trap is present, the data should also be inconsistent with the thermal model, in that a unique temperature cannot be derived from both channel ratios.

3. DISCUSSION

Of the six coronal flare sources listed in Table 1, two are consistent with impulsive phase coronal trapping in the thick-thin target scenario (1992 January 13 and 1993 November 30), and one is consistent with coronal trapping in the purely thin-target scenario (1993 February 17), although in the 1993 February 17 event the errors are sufficiently large that the data do not strongly support or contradict the trapping model (this may be a reflection of the complicated geometry of this event). The collisionally dominated trap model is rejected for the remaining three events, because the coronal spectrum is either softer than the assumed injected spectrum (inferred from the footpoints) or traverses the corona unmodified. The flare of 1991 November 19 yields the same "broken" power law (see Lin & Schwartz 1987) in the corona and footpoint regions, assuming a thin-target and thick-target approximation, respectively. This suggests that a single population of accelerated electrons is responsible for the coronal and chromospheric HXR emission. The 1992 October 4 flare can be readily described by a thermal model for the coronal emission, with a temperature of $\sim$30–40 MK.

The event of 1992 February 17 also demonstrates evidence of a "broken" power law at the loop footpoints but a softer spectrum in the coronal portion of the loop. This would suggest that an initially soft accelerated electron distribution is hardened as it passes through the corona. For this case the corona cannot be a simple thin target but must result in some modification of the spectrum. Such a spectral hardening might be obtained via energy losses due to Coulomb collisions ($dE/dt \propto E^{-1/2}$) as the particles traverse a high-density corona (see Fletcher 1995). Another interesting possibility for this event is the presence of a coronal trap with enhanced pitch angle scattering resulting in the *strong diffusion limit* of Kennel & Petschek (1966). In this case, the trapping time is directly proportional to the loop transit time (the bounce time), which scales with the inverse of the velocity ($t_{\rm trap} \propto E^{-1/2}$). Analogously to the discussion about the energy dependence of the weak diffusion trap (see Appendix), we would expect to infer an electron spectral index of 0.5 powers softer from the coronal regions than from the footpoint regions. This is consistent with the results for the flare of 1992 February 17.

Three of the events selected for this study were shown by Aschwanden et al. (1997) to be consistent with trapping of coronal electrons through energy-dependent time delays of $\sim$20–200 keV HXR emission (1992 January 13, February 17, and October 4). However, the time-delay analysis is subject to some uncertainty because time delays and spectral changes cannot, in general, be distinguished when the time structure is unknown (Aschwanden et al. 1997; LaRosa & Shore 1998; Brown et al. 1998). Hence, an independent test of the trapping scenario for the flares observed by Aschwanden et al. (1997) is essential.

Interestingly, only one of these three flares studied by Aschwanden et al. is consistent with a coronal trap in the weak diffusion limit (1992 January 13). The other events, 1992 February 17 and October 4, are consistent with a thin-target nonthermal emission and thermal bremsstrahlung production in the corona, respectively, with the spectrum of the coronal particle population being significantly softer than that inferred from the footpoints (Table 1). Hence, the data are inconsistent with the trap model in the weak diffusion limit, although the 1992 February 17 event may be consistent with trapping in the strong diffusion limit. This can be reconciled with the Aschwanden et al. timing results through a number of mechanisms. If a trap is not present in the corona, the Aschwanden et al. time delays would indicate either spectral changes in the accelerated electrons with time or a two-step acceleration process. A two-step acceleration process requires an overabundance of lower energy electrons relative to higher energy electrons, and this is not observed in the 1992 February 17 flare, although the error bars are large: the coronal LO/M1 ratio gives a harder spectrum than the M1/M2 ratio. Unfortunately, the time resolution of the HXT images is not sufficient to distinguish between these various possibilities.

All three of the events that are consistent with the trapping hypothesis require that the trap have sufficient density to significantly affect the lower energy electrons observed. In the thick-thin model, the energy at which the electron population transitions from "seeing" a thin target to "seeing" a thick target is given by

$$E_t = \sqrt{\left(\frac{N}{10^{20}\ {\rm cm}^{-2}}\right)\left(\frac{0.7}{\cos\ \alpha}\right)} \times 20\ {\rm keV}\ , \qquad (1)$$

where N is the column depth in the trap and α is the average pitch angle of the trapped electrons.

The response functions and energy discrimination of the HXT are such that an incident photon of 22.7 keV has equal probability of detection in either the LO or M1 channel.[3] In the flares that show evidence of a coronal trap (see Table 1), the inferred spectral indices determined from the two channel ratios can only be reconciled if the LO/M1 ratio results from thick-target emission and the M1/M2 ratio from thin-target emission. This suggests that the transition in photon energy occurs around 22.7 keV. The observation of such a break in the photon spectrum allows us to determine the electron energy at which the trap region changes from a thick to a thin target. For the cases discussed here, the electron spectrum dominates over the cross section for bremsstrahlung photon production and as a result the transition energy, $E_t \approx \epsilon_t$, where E_t denotes the electron energy and ϵ_t the photon energy at which the thick- to thin-target transition occurs. Therefore, for photon energies of $20 \leq \epsilon_t \leq 26$ keV (the range over which the LO and M1 channel detection thresholds overlap), we determine a range of most likely electron energies of $21 \leq E_t \leq 28$ keV. From equation (1) this implies that the electron density of the trap must be of order $1\text{–}2 \times 10^{11} L_9^{-1}$ cm^{-3}, where $L_9 = L/10^9$ cm and L is the spatial scale of the trap.

The thick-thin model therefore requires relatively high densities. We note that these values are generally consistent with those derived by Aschwanden et al. (1997) using energy-dependent time delays in the *CGRO* data. For the 1992 January 13, February 17, and October 4 flares, Aschwanden et al. calculate a density of 0.2×10^{11}, 2.89×10^{11}, and 3.7×10^{11} cm^{-3}, respectively. These values are generally consistent with the spectral observations through equation (1). However, as discussed above, we do not consider the 1992 February 17 or October 4 flares to be consistent with the trapping scenario.

The densities required for the thick-thin model seem high given that there is typically very little SXR emission from the HXR sources above the main SXR loop (Tsuneta et al. 1997). There are several solutions to this dilemma. First, a 1%–10% filling factor, where locally high densities are interspersed with lower densities, could make this possible; SXR emission would remain minimal, and the required modification of the electron spectrum would be possible. Alternatively, if the coronal source is due to electrons with pitch angles close to 90° (Fletcher 1995; Fletcher & Martens 1998), the electrons would remain in the corona for a relatively long time, and the effective length of the coronal source would be increased by a factor of $1/\cos \alpha$, where α is the average pitch angle. For this case, we would derive a more realistic density of 10^9 cm^{-3} when the pitch angle is in the range 84°–89°.

The implications of the trapping scenario are several. First, although it is clear that there are two particle populations present in the 1992 January 13 and 1993 February 17 and November 30 flares, both populations of energetic particles are consistent with a single injected energy spectrum and hence a single acceleration event, as the modified energy spectrum of the trapped population (coronal source) is consistent with the unmodified energy spectrum of the directly precipitating population (footpoint source). Thus, although two particle populations are required, there is likely to be a single acceleration mechanism for both populations. Second, in the flares observed here, the coronal HXR sources are due to the trapped particle population. The pervasiveness of the phenomenon (3/6 limb events) suggests that the magnetic field geometry in many flares is generally conducive to trapping in a confined region high in the corona, above the SXR loops.

The trapping of energetic electrons in a region above the SXR loop is predicted by the magnetic reconnection model of flares (e.g., Masuda et al. 1994; Shibata et al. 1995; Tsuneta et al. 1997). In this model, MHD slow-mode shocks attached to the reconnection region convert magnetic energy into plasma heating and into an outflow jet. The outflow jet forms a fast-mode shock just above the loop top SXR source. Energetic electrons are trapped in the HXR source between the slow-mode and fast-mode shocks. In a recent elaboration of this model, Tsuneta & Naito (1998) demonstrated how electrons can be accelerated through a first-order Fermi process at the fast shock. Hence, observations of the coronal trap above the SXR loop may be directly related to the particle acceleration process.

This model is consistent with the data presented here. Our data set requires that there be both a magnetic geometry conducive to particle trapping and a single acceleration mechanism responsible for both the trapped and the precipitating electron populations. The combination of the slow-mode and fast-mode shocks presents a natural trapping geometry at the required location just above the SXR loop. Further, if the particle acceleration is related to the presence of the fast-mode shock, as suggested by Tsuneta & Naito (1998), the trapped and the precipitating particle populations will be formed from a single acceleration process.

The spatial resolution of HXT is essential for the type of study carried out here, because the footpoint and coronal emission must be distinguished. However, the spectral resolution of HXT is only marginally able to demonstrate the existence of the coronal trapping in the thick-thin scenario. Further, the long temporal integrations required to reconstruct images with HXT means that it is difficult to observe the trap on timescales smaller than the trapping time. If possible, such an analysis would allow the measurement of the trap properties (see Appendix). In the near future, this type of analysis will be possible with the much better spectral and temporal resolution of the High-Energy Solar Spectroscopic Imager (HESSI) mission. With HESSI's superior spectral resolution, this type of analysis should be considerably more productive. It is clear from this study that it is spectral and temporal resolution, not spatial resolution, that is paramount, so long as the footpoint and coronal HXR emission can be distinguished.

4. CONCLUSIONS

The three flares discussed in this paper that are consistent with the trapping model lead us to a general picture of the Masuda-type flare. In each of these events, there are two populations of electrons present in the impulsive phase of the flares: the directly precipitating electrons observed at the flare footpoints and the trapped electrons observed in the corona, above the SXR loop. Because the loop-top source is formed by a population of trapped electrons and these trapped particles are consistent with a single acceleration of both the trapped and precipitating components, it is clear that the loop top source is nonthermal during the impulsive phase. Hence extreme temperatures, like the 120

[3] Photons above this energy have a higher probability of being detected in the M1 channel.

MK derived for the 1992 January 13 flare, are not required to explain the loop top sources. Finally, we note that because the loop-top source can be explained as a coronal trap, there must be a magnetic field geometry in the corona that is conducive to trapping, such as that suggested by Tsuneta & Naito (1998) or Fletcher & Martens (1998).

The *Yohkoh* Soft X-Ray Telescope is a collaborative project of the Lockheed Martin Solar and Astrophysics Laboratory, the National Astronomical Observatory of Japan, and the University of Tokyo, supported by NASA and ISAS.

APPENDIX

EFFECTS OF TRAPPING ON THE ELECTRON SPECTRUM

Integrating the electron spectrum over a data accumulation time and allowing for the escape of electrons from the coronal trap yields the electron spectrum, which would be derived from a HXR observation after the impulsive injection of electrons into a coronal trap, $\overline{F(E, t)}$:

$$\overline{F(E, t)} = \frac{1}{\Delta t} \int_{t_1}^{t_1 + \Delta t} F(E) \exp\left(\frac{-t}{t_{\rm trap}}\right) dt \,, \tag{A1}$$

where t_1 is the start time of the observation, relative to the time of the electron injection, Δt is the duration of the observation, $F(E)$ is the injected electron spectrum ($AE^{-\delta}$), and $t_{\rm trap}$ is the trapping time in the weak diffusion limit,

$$t_{\rm trap} = 0.95 \times 10^8 \left(\frac{E^{3/2}}{n_e}\right)\left(\frac{20}{\ln \Lambda}\right), \tag{A2}$$

where $t_{\rm trap}$ is in seconds, E is in keV, n_e is in cm^{-3}, and $\ln \Lambda$ is the Coulomb logarithm. Thus,

$$\overline{F(E, t)} = AE^{-\delta} \frac{t_{\rm trap}}{\Delta t} \left[1 - \exp\left(\frac{-\Delta t}{t_{\rm trap}}\right)\right] \exp\left(\frac{-t_1}{t_{\rm trap}}\right). \tag{A3}$$

For a short data accumulation time ($\Delta t \ll t_{\rm trap}$),

$$\overline{F(E, t)} = AE^{-\delta} \exp\left(-t_1/t_{\rm trap}\right), \tag{A4}$$

while for a long data accumulation time ($\Delta t \gg t_{\rm trap}$),

$$\overline{F(E, t)} = AE^{-\delta} \frac{t_{\rm trap}}{\Delta t} \exp\left(\frac{-t_1}{t_{\rm trap}}\right). \tag{A5}$$

As electrons escape the trap, the lower energy portion of the spectrum is truncated as a "cutoff" energy is introduced. This energy cutoff moves to higher energies with time; however, above the energy cutoff, the spectral index is essentially unchanged (Fig. 3).

For short accumulation times, the observations will show a spectral index given by the injected spectrum. Only for long data accumulation times do we see the proportionality between $\overline{F(E, t)}$ and $t_{\rm trap}$ and thus the additional (non–time-dependent) hardening of the spectrum by 1.5 powers (eq. [A2]). Note that if the HXR emission is sufficiently intense, imaging would be possible for ($\Delta t \ll t_{\rm trap}$), and the trapping time can be found from a ratio of the long and short observations:

$$\frac{\overline{F_{\rm long}(E, t)}}{\overline{F_{\rm short}(E, t)}} = \frac{t_{\rm trap}}{\Delta t_{\rm long}}. \tag{A6}$$

In the case of continuous injection of electrons into the coronal trap, the observed spectrum becomes

$$\overline{F(E, t)} = \frac{1}{\Delta t} \int_{t_1}^{t_1 + \Delta t} \int_0^t A(t') E^{-\delta(t')} \exp\left[-\frac{(t - t')}{t_{\rm trap}}\right] dt' \, dt \,, \tag{A7}$$

where A is now the injection *rate*. For a fixed injection profile [$A(t')$, $\delta(t')$ constant],

$$\overline{F(E, t)} = \frac{1}{\Delta t} \int_{t_1}^{t_1 + \Delta t} AE^{-\delta} t_{\rm trap} \left[1 - \exp\left(\frac{-t}{t_{\rm trap}}\right)\right] dt \tag{A8}$$

$$= AE^{-\delta} t_{\rm trap} \left\{1 - \frac{t_{\rm trap}}{\Delta t} \exp\left(\frac{-t_1}{t_{\rm trap}}\right)\left[1 - \exp\left(\frac{-\Delta t}{t_{\rm trap}}\right)\right]\right\}. \tag{A9}$$

This is illustrated in Figure 4. If Δt is considerably longer than a trapping time, or if the observation starts after several trapping times, the spectrum reaches a steady state,

$$\overline{F(E, t)} = AE^{-\delta} t_{\rm trap} \,, \tag{A10}$$

and we see the hardening of the spectrum by 1.5 powers. This is similar to the impulsive case, with $\Delta t \gg t_{\rm trap}$, except that there is no introduction of a cutoff energy with time.

After the steady state is reached, short and long data accumulations yield the same spectrum and it is not possible to determine the trapping time from the ratio of the long and short data accumulations as it was in the impulsive case. However, if the initial injection into the trap can be observed with a short data accumulation, when $\Delta t \ll t_{\rm trap}$ and $t_1 = 0$,

$$\overline{F(E, t)} = AE^{-\delta}\Delta t_{\rm short}\ , \tag{A11}$$

and, similar to equation (A6), we have

$$\frac{\overline{F_{\rm long}(E, t)}}{\overline{F_{\rm short}(E, t)}} = \frac{t_{\rm trap}}{\Delta t_{\rm short}}\ . \tag{A12}$$

REFERENCES

Alexander, D. 1990, A&A, 235, 431
Alexander, D., & Metcalf, T. 1997, ApJ, 489, 442 (AM97)
Aschwanden, M. J., Bynum, R. M., Kosugi, T., Hudson, H. S., & Schwartz, R. A. 1997, ApJ, 487, 936
Aschwanden, M., et al. 1996b, ApJ, 470, 1198
Aschwanden, M. J., Hudson, H. S., Kosugi, T., & Schwartz, R. A. 1996a, ApJ, 464, 985
Bai, T., & Dennis, B. R. 1985, ApJ, 292, 699
Bai, T., Hudson, H. S., Pelling, R. M., Lin, R. P., Scwartz, R. A., & von Rosenvinge, T. T. 1983, ApJ, 267, 443
Bai, T., & Ramaty, R. 1979, ApJ, 227, 1072
Brown, J. C., Conway, A. J., & Aschwanden, M. 1998, ApJ, 509, 911
Fletcher, L. 1995, A&A, 303, L9
Fletcher, L., & Martens, P. C. H. 1998, ApJ, 505, 418
Kennel, C. F., & Petschek, H. E. 1966, J. Geophys. Res., 71, 1
Kosugi, T., et al. 1991, Sol. Phys., 136, 17
LaRosa, T. N., & Shore, S. N. 1998, ApJ, 503, 429L
Lin, R. P., & Schwartz, R. A. 1987, ApJ, 312, 462
MacKinnon, A. L. 1988, A&A, 194, 279
Masuda, S., et al. 1994, Nature, 371, 495
———. 1995, PASJ, 47, 677
Metcalf, T. R., Hudson, H. S., Kosugi, T., Puetter, R. C., & Piña, R. K. 1996, ApJ, 466, 585
Ramaty, R., Schwartz, R. A., Enome, S., & Nakajima, H. 1994, ApJ, 436, 941
Sato, J., Kosugi, T., & Makishima, K. 1998, PASJ, in press
Shibata, K., Masuda, S., Shimojo, M., Hara, H., Yokoyama, T., Tsuneta, S., Kosugi, T., & Ogawara, Y. 1995, ApJ, 451, L83
Takakura, T., et al. 1993, PASJ, 45, 737
Tsuneta, S., Masuda, S., Kosugi, T., & Sato, J. 1997, ApJ, 478, 787
Tsuneta, S., & Naito, T. 1998, ApJ, 495, L67
Wheatland, M. S., & Melrose, D. B. 1995, Sol. Phys., 158, 283